Journal of Pharmaceutical Sciences 112 (2023) 3248–3255

Contents lists available at ScienceDirect

Journal of Pharmaceutical Sciences

journal homepage: www.jpharmsci.org

Lessons Learned

Optimization of Flow Imaging Microscopy Setting Using Spherical Beads with Optical Properties Similar to Those of Biopharmaceuticals

Takaaki Kurinomaru[a,*], Kimitoshi Takeda[a], Megumi Onaka[a], Yuki Kuruma[c], Keiji Takahata[c], Kayori Takahashi[c], Hiromu Sakurai[c], Akira Sasaki[d], Naohiro Noda[d], Shinya Honda[d], Risa Shibuya[b], Tomohiko Ikeda[b], Rio Okada[b], Tetsuo Torisu[b], Susumu Uchiyama[a,b,*]

[a] U-Medico Inc., 2-1 Yamadaoka, Suita, Osaka 565-0871, Japan
[b] Department of Biotechnology, Graduate School of Engineering, Osaka University, 2-1 Yamadaoka, Suita, Osaka 565-0871, Japan
[c] National Metrology Institute of Japan, National Institute of Advanced Industrial Science and Technology, 1-1-1 Umezono, Tsukuba, Ibaraki 305-8563, Japan
[d] Biomedical Research Institute, National Institute of Advanced Industrial Science and Technology, 1-1-1 Higashi, Tsukuba, Ibaraki 305-8566, Japan

ARTICLE INFO

Article history:
Received 12 June 2023
Revised 3 October 2023
Accepted 3 October 2023
Available online 7 October 2023

Keywords:
Biopharmaceutical
Flow imaging microscopy
Refractive index
Subvisible particle
Segmentation threshold

ABSTRACT

Flow imaging microscopy (FIM) is widely used to characterize biopharmaceutical subvisible particles (SVPs). The segmentation threshold, which defines the boundary between the particle and the background based on pixel intensity, should be properly set for accurate SVP quantification. However, segmentation thresholds are often subjectively and empirically set, potentially leading to variations in measurements across instruments and operators. In the present study, we developed an objective method to optimize the FIM segmentation threshold using poly(methyl methacrylate) (PMMA) beads with a refractive index similar to that of biomolecules. Among several candidate particles that were evaluated, 2.5-μm PMMA beads were the most reliable in size and number, suggesting that the PMMA bead size analyzed by FIM could objectively be used to determine the segmentation threshold for SVP measurements. The PMMA bead concentrations measured by FIM were highly consistent with the indicative concentrations, whereas the PMMA bead size analyzed by FIM decreased with increasing segmentation threshold. The optimal segmentation threshold where the analyzed size was closest to the indicative size differed between an instrument with a black-and-white camera and that with a color camera. Inter-instrument differences in SVP concentrations in acid-stressed recombinant adeno-associated virus (AAV) and protein aggregates were successfully minimized by setting an optimized segmentation threshold specific to the instrument. These results reveal that PMMA beads can aid in determining a more appropriate segmentation threshold to evaluate biopharmaceutical SVPs using FIM.

Introduction

Subvisible particles (SVPs), which are within the size range of 2–100 μm,[1,2] are a critical quality attribute in biopharmaceuticals, given that they can potentially affect the efficacy and safety of drug products.[3,4,5] Regulatory agencies have established stringent guidelines on the number of particles sized ≥10 μm and ≥25 μm, and compendial methods, such as light obscuration (LO) and microscopic particle count test, are typically used to assess SVPs.[6,7,8] In addition, characterization of SVPs sized <10 μm is required due to their potential immunogenicity.[9] Although risks associated with the SVPs of recently developed modalities, such as recombinant adeno-associated virus (AAV), are not well-known, assessing the SVPs of both novel and existing modalities is crucial in case of their unexpected safety risks.

Flow imaging microscopy (FIM) is a powerful technique to quantify and characterize SVPs in biopharmaceuticals.[10,11] Within the FIM instrument, particles are passed through an imaging field where they are illuminated by a light source for imaging at a maximum of 20× magnification with a charge-coupled device camera. Subsequently

* Correspondence authors at: 2-1 Yamadaoka, Suita, Osaka 565-0871, Japan.
E-mail addresses: kurinomaru.t@u-medico.co.jp (T. Kurinomaru), suchi@bio.eng.osaka-u.ac.jp (S. Uchiyama).

https://doi.org/10.1016/j.xphs.2023.10.007

performed automated image analysis provides morphological and numerical information, such as the particle size, count, and shape. FIM can characterize particle size and count for particles with a size range of approximately 1–400 μm and can assess shape for particles with a size range of approximately 5–400 μm.[12] Several reports have indicated that FIM is generally more sensitive than LO in detecting SVPs with a refractive index (*RI*) similar to that of biopharmaceuticals.[13-17] In recent years, machine learning has enabled the identification of various SVPs using FIM.[18,19]

Some FIM instruments allow users to customize capture settings to suit their particular needs and applications. One crucial factor in accurately capturing SVPs is the segmentation threshold, which establishes the boundary between the particle and the background based on the difference in the grayscale value of the pixels in captured images. If the segmentation threshold is set too high, some transparent particles can be excluded from the analysis and large particles can appear fragmented due to improper segmentation. Conversely, if the segmentation threshold is set too low, analytical data may include background noise and artifacts and oversizing may occur due to several factors such as the halo effect and edge gradient. In the FlowCam® instrument, the length of one pixel is approximately 0.6 μm at 10× magnification.[20] For SVPs sized ≤5 μm, which are less than a few tens of pixels in FlowCam®, selecting the optimal segmentation threshold is important because determining their size and count is particularly sensitive to this threshold value. However, developing an objective method to optimize the segmentation threshold has been challenging. Segmentation thresholds are often subjectively and empirically set based on values recommended in technical notes and literature or those determined in preliminary experiments. Using segmentation thresholds based on subjective and empirical criteria can lead to results that vary among different instruments and operators. For example, Kiyoshi et al. reported that variations in measurement results could still occur even if the segmentation threshold were standardized across several laboratories,[21] indicating that using the proper segmentation threshold might depend on the hardware configuration as well as the software settings. An alternative approach was reported by Cavicchi et al., who developed an imaging analysis algorithm to capture each particle with its corresponding segmentation threshold.[22] This approach also requires expertise, although an additional program allows for a more precise determination of the count and size. Therefore, methods to optimize the segmentation threshold without such programs have also been in demand.

One potential approach to overcome this roadblock is to use reference material to determine the segmentation threshold of the FIM instrument used for biomolecular SVPs. Polystyrene latex (PSL) beads are commonly used for the calibration of particle analysis. These beads have been used to adjust focus and perform a system suitability test for the verification of the sizing and counting accuracy of FIM instruments. However, the *RI* of PSL beads is higher than that of protein SVPs (1.59 vs. 1.41–1.46).[13,23] Due to their lower transparency stemming from a larger *RI* difference with the solvent, PSL beads are not preferred in optimizing the segmentation threshold for the measurement of more transparent SVPs. In practice, only the dark segmentation threshold is set for PSL beads whereas both the dark and light segmentation thresholds are set for more transparent SVPs (Fig. 1A). Therefore, it is preferable to use alternative reference materials with *RI*s that are closer to those of SVPs for segmentation threshold optimization. Among the several candidates developed to date, such as silica beads (*RI* = 1.41),[24] ethylene tetrafluoroethylene (ETFE; *RI* = 1.40),[25] and poly(methyl methacrylate) (PMMA) beads (*RI* = 1.49),[26] the latter are easier to handle because their density is lower than that of other candidate (approximately 1.2 g/mL vs. 2.0 and 1.7 g/mL for silica beads and ETFE, respectively)[25,26] and they are relatively water dispersible.

Semi-standardized materials are helpful to optimize segmentation thresholds for FIM measurements; their size and count should be precisely characterized and their *RI*s should be close to that of SVPs. We characterized the size and count of several candidate PMMA beads using the digital center distance finding (dCDF) method[27] and the mass-measurement-type optical particle counting (M-OPC) method,[28,29] respectively. Among these candidates, our preliminary data indicated that PMMA beads with a size of 2.5 μm passed very strict acceptance criteria, such as monodispersibility, sphericity, and storage stability. As shown in scanning electron microscopy images (Fig. 1B), these 2.5-μm PMMA beads are spherical and monodisperse. Although the size and concentration values in the present manuscript are indicative due to variations determined by uncertainty assessment (to be reported in the future), both the dCDF and M-OPC methods are Système International d'Unités traceable techniques, ensuring the reliability of the size and concentration of PMMA beads. In addition to the size and count accuracy, the *RI* of 2.5-μm PMMA beads (1.50)[30] is relatively close to that of SVPs. Therefore, we evaluated the potential utility of 2.5-μm PMMA beads as a potential reference material to determine optimal segmentation thresholds.

This study aimed to evaluate the feasibility of 2.5-μm PMMA beads for segmentation threshold optimization of FIM instruments. We found that PMMA bead concentrations measured using FIM were highly consistent with the indicative concentrations. We also found that the PMMA bead size analyzed by FIM decreased with increasing segmentation threshold. The optimal segmentation threshold where the analyzed size was close to the indicative size varied between an instrument equipped with a black-and-white camera and that equipped with a color camera. Inter-instrument differences in SVP concentrations of SVPs in acid-stressed AAV and protein aggregates were successfully minimized by setting an optimized segmentation threshold specific to each instrument. These results reveal that PMMA beads can aid users in determining more appropriate segmentation thresholds for the evaluation of biopharmaceutical SVPs.

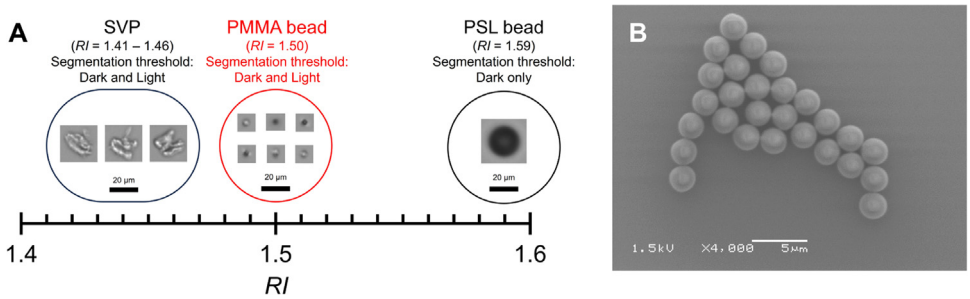

Figure 1. (A) Comparison of the refractive index (*RI*) values of subvisible particles (SVPs), polystyrene latex (PSL) beads, and poly(methyl methacrylate) (PMMA) beads. Representative images were obtained by FIM. (B) Scanning electron microscopic image of PMMA beads. Particles are uniform in size and highly spherical.

Table 1
Measurement settings for the FlowCam® instruments.

Measurement conditions	Instrument 1	Instrument 2
Hardware settings		
Cell depth (μm)	80	80
Cell width (μm)	700	700
Resolution (bit)	8	8
Camera	Black-and-white	Color
Focusing	Manual	Auto
Magnification	×10	×10
Software settings		
VisualSpreadsheet® software	Version 4.1.95	Version 4.17.14
Priming volume (mL)	0.25	0.25
Analyzed sample volume (mL)	0.15	0.15
Flow rate (mL/min)	0.05	0.05
Image capture rate (frames/s)	10	9
Efficiency (%)	71.5	71.5
Segmentation threshold (pixel)	Dark = 10–25, Light = 10–25	Dark = 10–27, Light = 10–27
Sizing parameter	ESD	ESD

Materials and Methods

Sample Preparation for Flow Imaging Microscopy

As raw material, an aqueous suspension of PMMA beads was purchased from Sekisui Kasei (Osaka, Japan). The mass concentration of the stock suspension was 1% according to the manufacturer's specification sheet. The stock suspension was diluted to 1×10^6 particles/mL with ultrapure water. A 20 mL aliquot of the suspension was placed in a polypropylene resin bottle which was sonicated in a sonication water bath (AS ONE, Osaka, Japan) for 2–5 min before the FIM measurement. Next, the solution was homogenized by placing the bottle on an orbital shaker at 150 rpm for 10 min at room temperature and then diluted with Milli-Q water.

AAV6-CMV-GFP encapsulating 2,500-base single-strand DNA was obtained from SignaGen Laboratories (Rockville, MD, USA). AAV vector stocks were prepared in phosphate-buffered saline (PBS) containing 0.005% poloxamer 188 to a titer value of 1×10^{13} vg/mL. The stock AAV6 was spiked into the control solution (PBS with 0.05 v/v% poloxamer 188, pH 7.4) or an acidic solution (19 mM citrate with 0.05 v/v% poloxamer 188, pH 3.0), followed by incubation overnight at room temperature until FIM measurements. The final AAV6 concentration was 1×10^{11} vg/mL.

Particle Analysis by Flow Imaging Microscopy

As shown in Table 1, two FlowCam 8100™ systems (Yokogawa Fluid Imaging Technologies, Scarborough, ME, USA) were used to perform FIM measurements. Instrument 1 was equipped with a black-and-white camera that required manual focusing, whereas Instrument 2 was equipped with a color camera that automatically adjusted focus. Before measurement, cleanliness test was performed using Milli-Q water, and system suitability test was performed using National Institute of Standard and Technology-certified PSL beads with a size of 20 μm (COUNT-CAL CC20; Thermo Fisher Scientific, Fremont, CA, USA). The image capture rate was set to 9–10 frames/s to obtain an efficiency value of >70%. The same segmentation threshold was used for both dark and light. Sample volumes of 0.15 mL were analyzed at a flow rate of 0.05 mL/min.

The VisualSpreadsheet® software (version 4.1.95 for Instrument 1; version 4.17.14 for Instrument 2; Yokogawa Fluid Imaging Technologies) was used to perform data analysis. By default, the instrument saves a collage image that segments particles from the raw camera image, enabling the deletion of the original raw camera image. In addition, the raw camera images were saved and reanalyzed to evaluate the effect of changes in the segmentation threshold on the size and concentration determined with FIM.

Results and Discussion

In the present study, we used 2.5-μm PMMA beads with high consistent size and count to optimize the segmentation thresholds for SVP measurements. To investigate the effect of hardware configurations on measurements, we used two FIM instruments, including one with a manual-focus black-and-white camera (Instrument 1) and one with an autofocus color camera (Instrument 2). We initially performed FIM measurements of PMMA beads on Instrument 1 using the general segmentation threshold recommended by the manufacturer (dark = 15, light = 15)[31]. Fig. 2 shows the relationship between

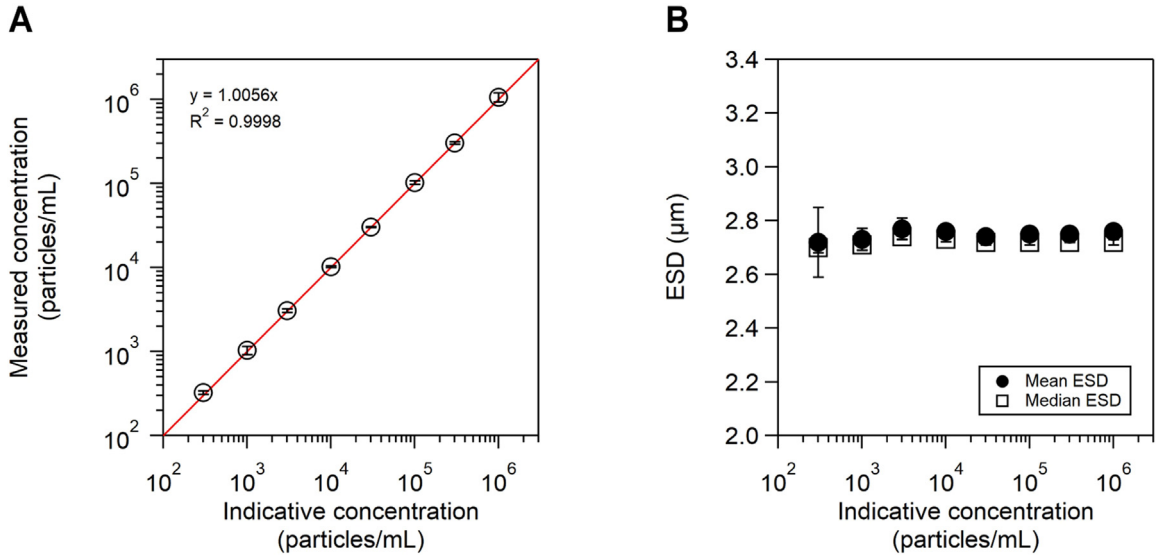

Figure 2. Correlation between the indicative and measured concentrations (A) and sizes (B) of PMMA beads. FIM measurements of 3×10^2–1×10^6 particles/mL of PMMA beads were performed five times on Instrument 1. Data were obtained from measurements conducted using different segmentation thresholds, with both dark and light pixel values set to 15. The red line shows that the indicative concentrations were equal to the measured concentrations. Data are shown as means ± standard deviation of the mean. The intensity mean of Instrument 1 was 154.

the indicative and measured PMMA bead concentrations. The measured total concentrations were highly consistent with the indicative values, and the bead sizes were similar independent of the indicative concentrations. The mean and median equivalent spherical diameters (ESDs) were nearly identical, indicating that the PMMA beads were monodisperse.

Given that the measured bead size determined using the general segmentation threshold (approximately 2.7 μm) was higher than the indicative size (2.5 μm), the PMMA bead size and count were determined by changing the segmentation threshold in increments of 5. As shown in Fig. 3A, the PMMA bead size decreased with increasing segmentation threshold whereas the total concentration remained similar. Since the segmentation threshold determines the boundary between the particle and the background according to the difference in pixel intensities, increasing the segmentation threshold might lead to a decrease in the size of individual PMMA beads. As shown in Fig. S1, setting a lower segmentation threshold led to a greater overestimation of the bead size due to the false detection of several factors, such as the halo effect or edge gradient. Compared with the relative SVP concentration in each size range (Fig. 3B), the concentrations of 2–3 μm particles were >90% when the segmentation threshold was set to 20. At this segmentation threshold, the average size was closest to the indicative value and the concentration of 2–3 μm particles was the highest, indicating that the optimal segmentation threshold was nearly 20 for Instrument 1.

Next, we perform FIM measurements of PMMA beads in two different FlowCam® instruments to determine whether the optimal segmentation threshold was dependent on the specific hardware configuration of the FIM instrument. Fig. 4 shows the sizes and total concentrations of PMMA beads determined by each instrument. Similar to Instrument 1, the bead size measured by Instrument 2 decreased with increasing segmentation threshold whereas the concentration remained nearly constant regardless of the segmentation threshold. The segmentation threshold that resulted in the size closest to the indicative size of 2.5 μm was different between the two instruments (20 and 25 for Instrument 1 and 2, respectively). Color cameras have lower spatial resolution than black-and-white cameras,[20] which can result in less accurate determination of particle size near the lower limit of approximately 2 μm at 10× magnification. These results suggested that the optimal segmentation threshold was specific for each detection camera and could be determined with the measurement of PMMA beads.

The total concentration determined in the experiment shown in Fig. 4A slightly decreased as a function of the segmentation threshold, whereas the total concentration determined in the experiment shown in Fig. 3 did not change although Instrument 1 was used in

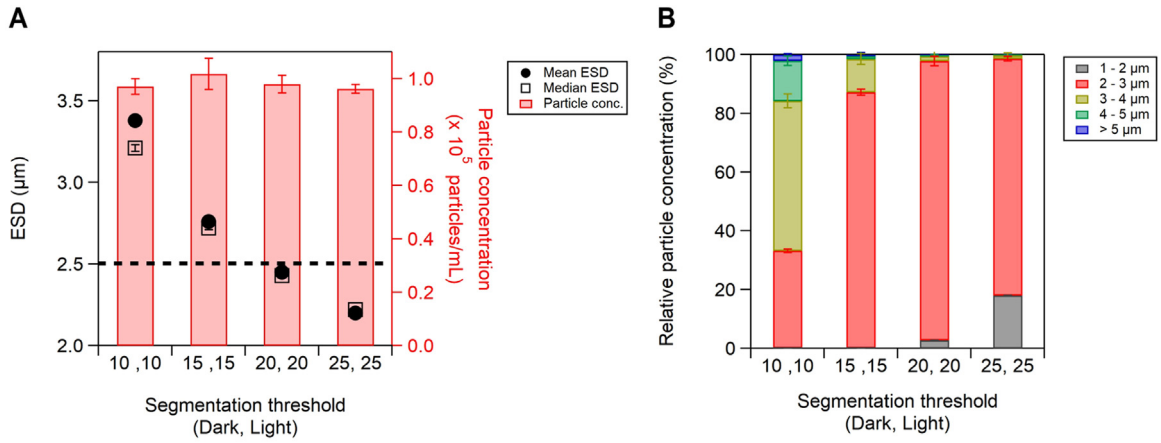

Figure 3. Size and total concentration (A) and relative concentration of particles in each size range (B) in PMMA bead solution measured using indicated segmentation thresholds. FIM measurements of 1×10^5 particles/mL of PMMA beads were performed three times on Instrument 1. Data were obtained from measurements conducted using different segmentation thresholds, with both dark and light pixel values set to 10–25. The black dashed line represents the indicative size (2.5 μm). Data are shown as means ± standard deviation of the mean. The intensity mean of Instrument 1 was 154.

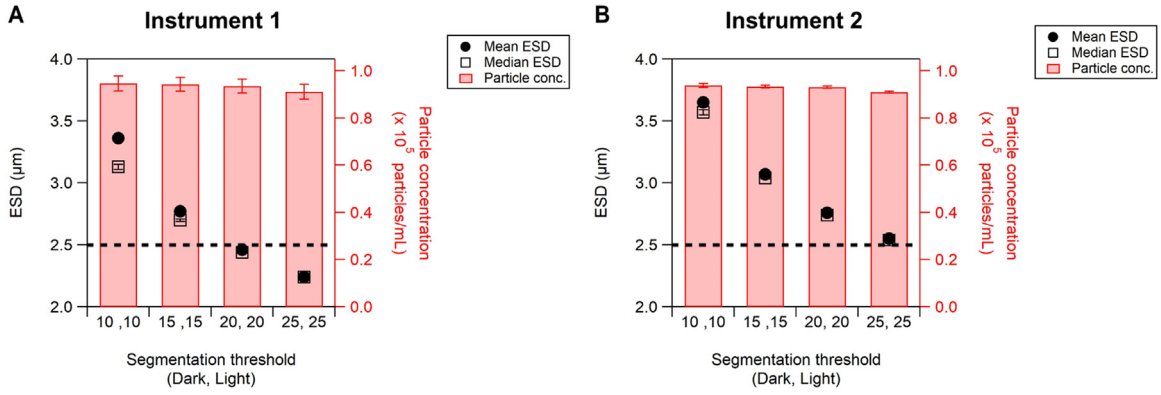

Figure 4. Comparison of the measured size and total concentration of particles between the two FlowCam® instruments used in this study. FIM measurements of 1×10^5 particles/mL of PMMA beads were performed three times on Instruments 1 (A) and 2 (B). Data were obtained by reanalyzing raw camera images using different segmentation thresholds, with both dark- and light-pixel values ranging from 10 to 25. Black dashed lines represent the indicative size (2.5 μm). Data are shown as means ± standard deviation of the mean. The intensity means of Instruments 1 and 2 were 154 and 156, respectively.

Table 2
PMMA bead size and total concentrations determined by Instrument 1 with different segmentation thresholds.

Segmentation threshold	Mean ESD (μm)	Median ESD (μm)	Total concentration (particles/mL)
Dark = 10, Light = 10	3.38 ± 0.03	3.21 ± 0.02	96,964 ± 2,975
Dark = 15, Light = 15	2.76 ± 0.02	2.72 ± 0.01	101,740 ± 5,810
Dark = 20, Light = 20	2.45 ± 0.01	2.43 ± 0.01	97,847 ± 3,267
Dark = 25, Light = 25	2.20 ± 0.01	2.22 ± 0.01	96,107 ± 1,641

Data were obtained from each measurement with different segmentation thresholds, with both dark and light pixel values set to 10–25.

both experiments (Tables 2 and 3). The decrease in total particle concentration with increasing segmentation threshold was clearer as the PMMA bead concentration decreased (Fig. S2). The data in Fig. 4A were obtained by reanalyzing the raw camera images, and the same image sets with different segmentation thresholds were used to calculate the total concentrations. Increasing the segmentation threshold hindered the ability to distinguish the boundary of 1–2 μm particles and the background with the magnification of the camera in Instrument 1. Consequently, increasing the segmentation threshold could have caused a decrease in the count of apparent 1–2 μm particles such as particles flowing out of focus. In contrast, the data in Fig. 3 were obtained from multiple measurements with Instrument 1. Since individual image sets were used to calculate the concentration, the total concentrations were not affected by changes in the segmentation threshold.

To explore more appropriate segmentation thresholds in which PMMA size is closer to the indicative value, the PMMA bead size and count were determined by changing the segmentation threshold in increments of 1, starting from 20 for Instrument 1 and 25 for Instrument 2. As shown in Tables 4 and 5, the analyzed ESDs were close to 2.5 μm when the segmentation thresholds were set to 19 and 26 for Instruments 1 and 2, respectively. In addition, curve fitting was performed for the data in which PMMA bead size was determined by changing the segmentation threshold in increments of 5 (10, 15, 20, and 25) as an alternative method to optimize the segmentation threshold. Four simple functions (linear, exponential, logarithmic, and power) were selected for curve fitting, and the estimated ESD values by the curve fitting and the analyzed ESD values by the Visual-

Table 3
Total PMMA bead concentrations determined by Instruments 1 and 2 with different segmentation thresholds.

Segmentation threshold	Total concentration (particles/mL)	
	Instrument 1	Instrument 2
Dark = 10, Light = 10	94,614 ± 3,117	93,844 ± 838
Dark = 15, Light = 15	94,340 ± 2,920	93,314 ± 631
Dark = 20, Light = 20	93,611 ± 2,900	93,080 ± 514
Dark = 25, Light = 25	91,145 ± 3,169	91,075 ± 329

Data were obtained by reanalyzing raw camera images using different segmentation thresholds, with both dark and light pixel values ranging from 10 to 25.

Table 4
PMMA bead size analyzed by VisualSpreadsheet® software for Instrument 1 and estimated by curve fitting.

Segmentation threshold	Mean ESD (μm)		Median ESD (μm)	
	Analyzed value	Estimated value	Analyzed value	Estimated value
18	2.57 ± 0.01	2.58	2.53 ± 0.01	2.53
19	2.52 ± 0.01	2.52	2.48 ± 0.01	2.48
20	2.46 ± 0.01	2.46	2.44 ± 0.01	2.43
21	2.41 ± 0.01	2.41	2.39 ± 0.01	2.39

Table 5
PMMA bead size analyzed by VisualSpreadsheet® software for Instrument 2 and estimated by curve fitting.

Segmentation threshold	Mean ESD (μm)		Median ESD (μm)	
	Analyzed value	Estimated value	Analyzed value	Estimated value
24	2.59 ± 0.02	2.58	2.57 ± 0.01	2.56
25	2.55 ± 0.02	2.54	2.54 ± 0.00	2.52
26	2.52 ± 0.02	2.50	2.50 ± 0.02	2.49
27	2.49 ± 0.02	2.46	2.46 ± 0.01	2.45

Spreadsheet® software were compared. Among them, the power was the best-fitted function with the highest R_2 (Fig. S3), and the estimated ESDs derived from this equation were comparable to the analyzed values (Tables 4 and 5). These results suggested the utility of curve fitting in segmentation threshold optimization.

Proper assessment of SVPs in virus- and liquid nanoparticle-based pharmaceuticals is required to ensure drug safety and efficacy. Thus, we chose AAV as a model biopharmaceutical with an estimated *RI* value of 1.43–1.50)[32,33] and a measured *RI* of 1.43 (Fig. S4), close to that of 2.5-μm PMMA beads. To resemble the stress that might occur during manufacturing, AAV samples were treated with acid stress overnight, leading to AAV denaturation and particle formation. Fig.s 5A and 5C show the SVP concentration in each size range in the AAV solution determined by Instrument 1. The total concentration of both control and acid-stressed AAV decreased with increasing segmentation threshold. Fig. 5E shows the relative SVP concentration in each size range with specific segmentation thresholds used to measure the acid-stressed AAV. The concentration patterns were similar to measurements using segmentation thresholds between 15 and 25, whereas the concentration pattern determined with a segmentation threshold of 10 differed from those determined using other segmentation thresholds. Similar results were obtained with Instrument 2 (Fig. 5B, 5D, 5F).

Although few studies reported the size of AAV SVPs, AAV is less likely to form large SVPs compared to common protein SVPs. The SVPs of the shear-stressed protein aggregates contained many particles that were 3–4 and 4–5 μm in size (Fig. S5), whereas the SVPs of the acid-stressed AAV contained few particles in this range (Fig. 5E, 5F). Hiemenz et al. reported that heat-stressed AAV contained more SVPs sized ≤4 μm and fewer SVPs sized >4 μm.[34] Interestingly, the concentration of SVPs detected by FIM decreases with increasing dilution of heat-stressed AAV, suggesting that large SVP might dissociate by dilution.[34] Although AAV SVPs require further investigation, it may be reasonable to use 2.5-μm PMMA beads to optimize the segmentation threshold for AAV SVP analysis since PMMA beads are close to the size range of major AAV SVPs.

The indicative size of 2.5-μm PMMA beads was reliable, and their *RI* value was close to that of biopharmaceutical SVPs; therefore, the segmentation threshold for AAV measurements can be optimized based on the measured ESD of PMMA beads. As shown in Tables 4 and 5, the ESD value was close to 2.5 μm when the segmentation threshold was set to 19 and 26 for Instruments 1 and 2, respectively. Compared to the results obtained using a general segmentation threshold (dark = 15, light = 15), the particle concentration in acid-stressed AAV determined using the optimized segmentation threshold was consistently similar between the two instruments (Fig. 6, Table 6). Similar to AAV, using the optimized segmentation threshold resulted in consistent SVP concentrations of protein aggregates between the two instruments (Fig. S6, Table S1). Thus, segmentation threshold optimization with PMMA beads can reduce variations in particle concentration across different instruments.

The optimized segmentation thresholds were higher than those recommended by the manufacturer.[31] Higher segmentation thresholds might lead to the exclusion of more transparent SVPs from the

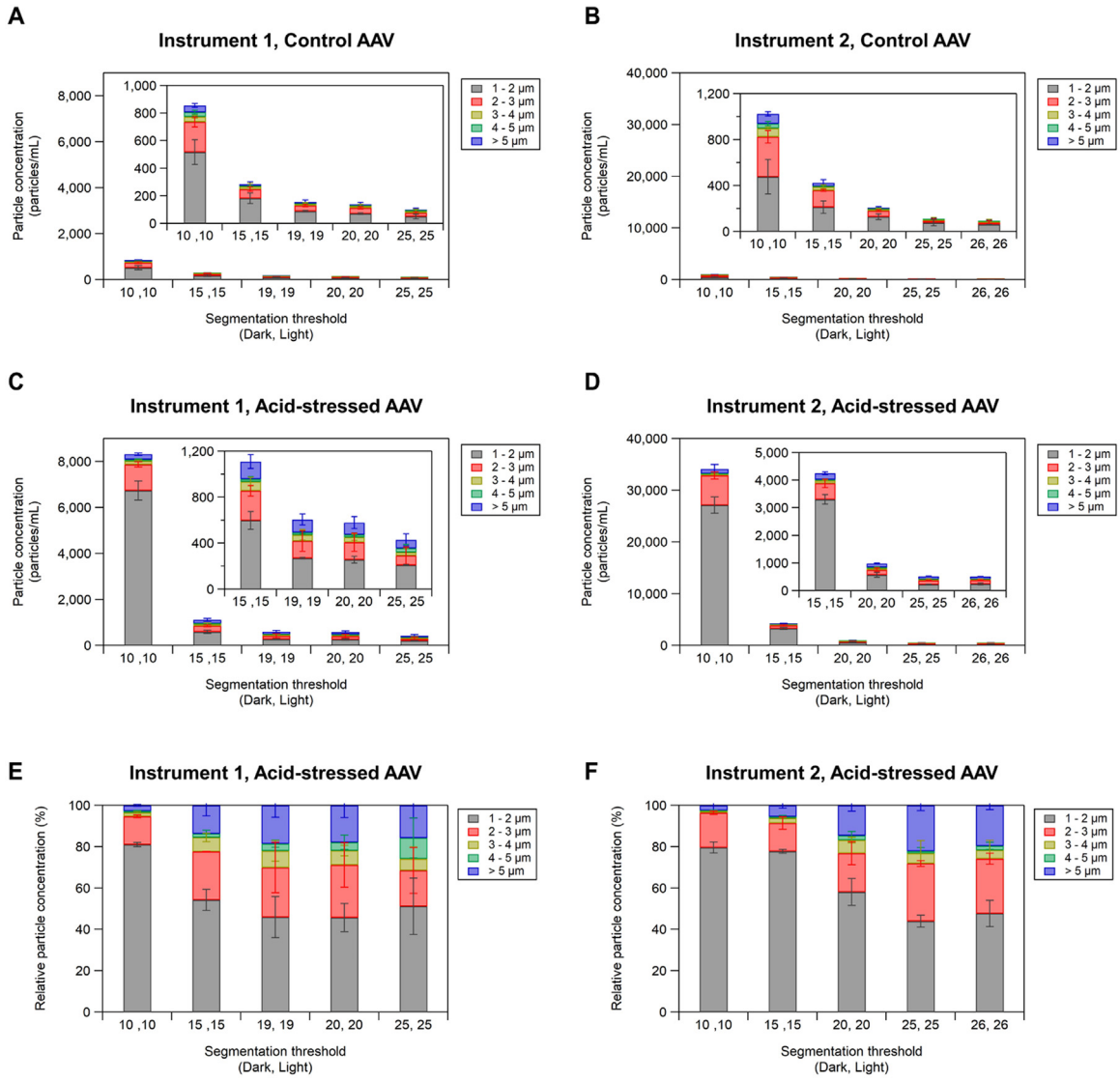

Figure 5. (A–D) SVP concentration in each size range in adeno-associated virus (AAV) solution determined using different segmentation thresholds. FIM measurements of 1×10^{11} vg/mL of control AAV (A, B) and acid-stressed AAV (C, D) were performed three times separately on Instruments 1 (A, C) and 2 (B, D). Data were obtained by reanalyzing raw camera images using different segmentation thresholds, with both dark- and light-pixel values ranging from 10 to 26. (E, F) Relative SVP concentration of each size range in acid-stressed AAV determined with different segmentation thresholds using Instruments 1 (E) and 2 (F). The intensity means of Instruments 1 and 2 were 153 and 156, respectively.

analysis, and large particles may become fragmented due to improper segmentation. However, setting a segmentation threshold lower than the optimized value increases the risk of erroneously detecting background noise or artifacts and can cause oversizing due to several factors, such as the halo effect and edge gradient. While the method proposed by Cavicchi et al., which uses an imaging analytical algorithm to determine the appropriate segmentation threshold for each particle, is likely to yield more accurate particle measurements,[22] our method of segmentation threshold optimization using PMMA beads offers a potentially simpler and more objective approach to determine the segmentation thresholds for SVPs in biopharmaceuticals, resulting in the minimization of inter-instrumental variations.

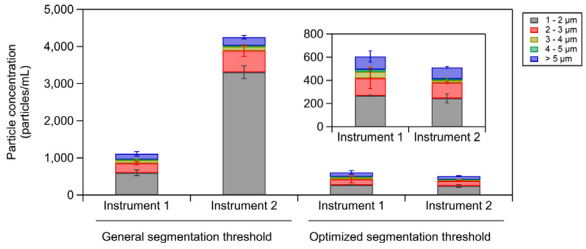

Figure 6. The concentration of SVPs in each size range in acid-stressed AAV solution determined using general (dark = 15, light = 15) or optimized (dark = 19, light = 19 for Instrument 1; dark = 26, light = 26 for Instrument 2) segmentation thresholds

PMMA beads are expected to apply for not only other FIM instruments including MFI (ProteinSimple, San Jose, CA, USA) and iSpect (Shimadzu, Kyoto, Japan) but also other particle analytical techniques, such as dynamic/static light scattering, quantitative laser diffraction, three-dimensional homodyne light detection, and LO.[23,35] For example, Matter et al. reported the impact of two different calibration materials with their *RI* differences (ΔRIs) between standard beads and solvents for particle analysis using LO and MFI.[24] PSL beads in water (ΔRI = 0.26) and SiO_2 beads in sucrose (ΔRI = 0.06) were used as calibration materials, latter ΔRI was similar to that between protein particles and the formulation buffer. The protein particle counts determined by LO and MFI changed depending on the

Table 6
SVP concentration in acid-stressed AAV determined using general and optimized segmentation thresholds.

Segmentation threshold	Instrument	Particle concentration in acid-stressed AAV (particles/mL)					
		1–2 μm	2–3 μm	3–4 μm	4–5 μm	>5 μm	Total
Dark = 15 Light = 15	Instrument 1	598 ± 77	259 ± 46	79 ± 38	22 ± 20	152 ± 60	1110 ± 194
Dark = 15 Light = 15	Instrument 2	3308 ± 171	582 ± 157	104 ± 9	31 ± 27	229 ± 50	4254 ± 251
Dark = 19 Light = 19	Instrument 1	268 ± 6	151 ± 89	53 ± 45	21 ± 10	113 ± 48	606 ± 156
Dark = 26 Light = 26	Instrument 2	244 ± 39	135 ± 9	21 ± 24	11 ± 9	100 ± 8	510 ± 19

General segmentation threshold: dark = 15, light = 15.
Optimized segmentation threshold: dark = 19, light = 19 for Instrument 1; dark = 26, light = 26 for Instrument 2.

calibration material, although the changes were greater with LO than with MFI. One drawback of SiO_2 beads is their tendency to quickly sediment due to high density, leading to significant discrepancies in particle concentrations. Similarly, during our selection of PMMA bead candidates, we observed that beads sized ≥10 μm exhibited greater variation in measured concentrations compared to the 2.5-μm PMMA beads (data not shown), likely due to the faster sedimentation rate. Considering several advantages such as monodispersity, accuracy in size and concentration, *RI*, and water dispersibility, 2.5-μm PMMA beads are feasible for various particle analyses.

Of note, the optimized segmentation thresholds were determined under the specific light intensity mean of each instrument (Instrument 1, 153–154; Instrument 2, 156). because the measured size and concentration of PMMA beads changed in parallel with the change in the light intensity mean (Fig. S7). The combination of segmentation threshold with intensity mean is important for accurate quantification, and PMMA beads are well suited to optimize the combination. In addition, our studies revealed that the concentration of PMMA beads measured by an FIM instrument with a dirty flow cell was lower than that determined using the same instrument with a clean flow cell (data not shown), suggesting that cleanliness checks using PMMA beads were sensitive to the flow cell cleanliness. The feasibility of 2.5-μm PMMA beads as a reference material for other applications should be evaluated in future studies.

Conclusion

In the present study, we evaluated the utility of 2.5-μm PMMA beads as a potential reference material for segmentation threshold optimization during the characterization of biopharmaceutical SVPs using FlowCam® instruments. An optimized threshold could be determined based on the FIM measurement of PMMA beads, resulting in minimizing the inter-instrument variations of SVP concentration. Of note, the optimization of the segmentation threshold by size comparison could be achieved only using very accurately sized PMMA beads. We also demonstrated that the choice of segmentation threshold had a significant effect on the particle counting and sizing of AAV and protein aggregates, underscoring the importance of using reference material to determine the appropriate segmentation threshold. Expanding the feasibility of PMMA beads as a reference material requires additional studies.

Declaration of Competing Interest

The authors declare that they have no conflicts of interest.

Acknowledgments

Funding: This study was supported by a grant-in-aid from the "Research and development of core technologies for gene and cell therapy" supported by the Japan Agency for Medical Research and Development (AMED) (grant number JP18ae0201001, JP18ae0201002). The authors thank Sekisui Kasei for supplying the PMMA particles. We thank Kumiko Yokogawa and Hiroe Sasaki at U-Medico Inc. for their assistance with the FIM measurement.

Supplementary Materials

Supplementary material associated with this article can be found in the online version at doi:10.1016/j.xphs.2023.10.007.

References

1. Narhi LO, Corvari V, Ripple DC, Afonina N, Cecchini I, Defelippis MR, et al. Subvisible (2-100 μm) particle analysis during biotherapeutic drug product development: Part 1, considerations and strategy. *J Pharm Sci*. 2015;104(6):1899–1908.
2. Corvari V, Narhi LO, Spitznagel TM, Afonina N, Cao S, Cash P, et al. Subvisible (2-100 μm) particle analysis during biotherapeutic drug product development: Part 2, experience with the application of subvisible particle analysis. *Biologicals*. 2015;43(6):457–473.
3. Carpenter JF, Randolph TW, Jiskoot W, Crommelin DJ, Middaugh CR, Winter G, et al. Overlooking subvisible particles in therapeutic protein products: gaps that may compromise product quality. *J Pharm Sci*. 2009;98(4):1201–1205.
4. Singh SK, Afonina N, Awwad M, Bechtold-Peters K, Blue JT, Chou D, et al. An industry perspective on the monitoring of subvisible particles as a quality attribute for protein therapeutics. *J Pharm Sci*. 2010;99(8):3302–3321.
5. Roberts CJ. Protein aggregation and its impact on product quality. *Curr Opin Biotechnol*. 2014;30:211–217.
6. United States Pharmacopoeia. <787>Sub-visible particulate matter in therapeutic protein injections. 2014:663-665.
7. United States Pharmacopeia. <788>Particulate matter in injections. 2014:398-401.
8. 2.9.19 Particulate contamination. Sub-visible particles. *Eur Pharmacopoeia*. 2021:4785–4787.
9. *Guidance for Industry: Immunogenicity Assessment for Therapeutic Protein Products*. FDA; 2014.. Available at: https://www.fda.gov/media/85017/download. Accessed August 17, 2021.
10. Sharma DK, King D, Oma P, Merchant C. Micro-flow imaging: flow microscopy applied to sub-visible particulate analysis in protein formulations. *AAPS J*. 2010;12(3):455–464.
11. Wuchner K, Büchler J, Spycher R, Dalmonte P, Volkin DB. Development of a microflow digital imaging assay to characterize protein particulates during storage of a high concentration IgG1 monoclonal antibody formulation. *J Pharm Sci*. 2010;99(8):3343–3361.
12. Brown L. Rapid particle size and shape characterization using continuous digital imaging. In: *Proceedings of the PMCA 61st Annual Production Conference*. 2007. April 16-18.
13. Zölls S, Gregoritza M, Tantipolphan R, Wiggenhorn M, Winter G, Friess W, et al. How subvisible particles become invisible-relevance of the refractive index for protein particle analysis. *J Pharm Sci*. 2013;102(5):1434–1446.
14. Demeule B, Messick S, Shire SJ, Liu J. Characterization of particles in protein solutions: reaching the limits of current technologies. *AAPS J*. 2010;12(4):708–715.
15. Werk T, Volkin DB, Mahler HC. Effect of solution properties on the counting and sizing of subvisible particle standards as measured by light obscuration and digital imaging methods. *Eur J Pharm Sci*. 2014;53:95–108.
16. Yoneda S, Niederleitner B, Wiggenhorn M, Koga H, Totoki S, Krayukhina E, et al. Quantitative laser diffraction for quantification of protein aggregates: comparison with resonant mass measurement, nanoparticle tracking analysis, flow imaging, and light obscuration. *J Pharm Sci*. 2019;108(1):755–762.
17. Shibata H, Harazono A, Kiyoshi M, Ishii-Watabe A. Quantitative evaluation of insoluble particulate matters in therapeutic protein injections using light obscuration and flow imaging methods. *J Pharm Sci*. 2022;111(3):648–654.

18. Gambe-Gilbuena A, Shibano Y, Krayukhina E, Torisu T, Uchiyama S. Automatic identification of the stress sources of protein aggregates using flow imaging microscopy images. *J Pharm Sci*. 2020;109(1):614–623.
19. Nishiumi H, Deiringer N, Krause N, Yoneda S, Torisu T, Menzen T, et al. Utility of three flow imaging microscopy instruments for image analysis in evaluating four types of subvisible particle in biopharmaceuticals. *J Pharm Sci*. 2022;111(11):3017–3028.
20. Yokogawa fluid imaging technologies, Inc. Available at: https://info.fluidimaging.com/hubfs/Documents/Tech%20Briefs/Color%20vs.%20BW%20Camera.pdf?hsLang=en. Accessed March 31, 2023.
21. Kiyoshi M, Shibata H, Harazono A, Torisu T, Maruno T, Akimaru M, et al. Collaborative study for analysis of subvisible particles using flow imaging and light obscuration: experiences in Japanese biopharmaceutical consortium. *J Pharm Sci*. 2019;108(2):832–841.
22. Cavicchi RE, Collett C, Telikepalli S, Hu Z, Carrier M, Ripple DC. Variable threshold method for determining the boundaries of imaged subvisible particles. *J Pharm Sci*. 2017;106(6):1499–1507.
23. Totoki S, Yamamoto G, Tsumoto K, Uchiyama S, Fukui K. Quantitative laser diffraction method for the assessment of protein subvisible particles. *J Pharm Sci*. 2015;104(2):618–626.
24. Matter A, Koulov A, Singh S, Mahler HC, Reinisch H, Langer C, et al. Variance between different light obscuration and flow imaging microscopy instruments and the impact of instrument calibration. *J Pharm Sci*. 2019;108(7):2397–2405.
25. Ripple DC, Montgomery CB, Hu Z. An interlaboratory comparison of sizing and counting of subvisible particles mimicking protein aggregates. *J Pharm Sci*. 2015;104(2):666–677.
26. Benkstein KD, Balakrishnan G, Bhirde A, Chalus P, Das TK, Do N, et al. An interlaboratory comparison on the characterization of a sub-micrometer polydisperse particle dispersion. *J Pharm Sci*. 2022;111(3):699–709.
27. Kuruma Y, Sakaguchi T, Takahata K, Sakurai H. Accurate size measurement of spherical particles using digital center distance finding method. *Abstract of Autumn Meeting of the Society of Powder Technology*. Tokyo, Japan; 2022. Dec. 6-7.
28. Kuruma Y, Sakaguchi T, Sakurai H. Mass-measurement-type optical particle counting method for determination of number concentration of liquid-borne particles. *Adv Powder Technol*. 2020;31(2):848–858.
29. Kuruma Y, Sakaguchi T, Sakurai H. Primary standard for the number concentration of liquid-borne particles: extension of the diameter range from the micrometer to the sub-micrometer level and reduction of the measurement uncertainty. *Metrologia*. 2021;58: 045007. (13pp).
30. Takahashi K, Kuruma Y, Takahata K, Sakurai H. Determination of refractive index increments of PMMA particles dispersed in liquid phase. *Adv Powder Technol*. 2023;34(10): 104185.
31. Yokogawa fluid imaging technologies, Inc. Available at: https://info.fluidimaging.com/hubfs/flowcam-8000-series-configuration-guide.pdf. Accessed March 31, 2023.
32. Zhang X, Wang W, Kenrick S, AN5007: characterization of AAV-based viral vectors by DynaPro DLS/SLS instruments. http://wyattfiles.s3.amazonaws.com/literature/app-notes/dls-plate/AN5007-AAV-quantitation-and-stability-analysis-by-batch-DLS.pdf. Accessed March 31, 2023.
33. Cole L, Fernandes D, Hussain MT, Kaszuba M, Stenson J, Markova N. Characterization of recombinant Adeno-Associated Viruses (rAAVs) for gene therapy using orthogonal techniques. *Pharmaceutics*. 2021;13(4):586.
34. Hiemenz C, Pacios-Michelena A, Helbig C, Vezocik V, Strebl M, Nikels F, et al. Characterization of virus particles and submicron-sized particulate impurities in recombinant adeno-associated virus drug product. *J Pharm Sci*. 2023;112(8):2190–2202.
35. Fukuhara A, Anzai Y, Osawa K, Umeda M, Minemura H, Shiramizu N, et al. Plate reader-based analytical method for the size distribution of submicron-sized protein aggregates using three-dimensional homodyne light detection. *J Pharm Sci*. 2021;110(12):3803–3810.